An Ensemble Forecast of the South China Sea Monsoon[①]

T. N. Krishnamurti, Mukul Tewari, Ed Bensman, Wei Han, Zhan Zhang,

Department of Meteorology, Florida State University, Tallahassee, FL 32306–4250

William K. M. Lau

Climate and Radiation Branch, Code 913, NASA Goddard Space Flight Center Greenbelt, MD 20771

ABSTRACT

This paper presents a generalized ensemble forecast procedure for the tropical latitudes. Here we propose an empirical orthogonal function–based procedure for the definition of a seven–member ensemble. The wind and the temperature fields are perturbed over the global tropics. Although the forecasts are made over the global belt with a high–resolution model, the emphasis of this study is on a South China Sea monsoon. Over this domain of the South China Sea includes the passage of a Tropical Storm, Gary, that moved eastwards north of the Philippines. The ensemble forecast handled the precipitation of this storm reasonably well. A global model at the resolution Triangular Truncation 126 waves is used to carry out these seven forecasts. The evaluation of the ensemble of forecasts is carried out via standard root mean square errors of the precipitation and the wind fields. The ensemble average is shown to have a higher skill compared to a control exper- iment, which was a first analysis based on operational data sets over both the global tropical and South China Sea domain. All of these experiments were subjected to physical initialization which provides a spin–up of the model rain close to that obtained from satellite and gauge–based esti- mates. The results furthermore show that inherently much higher skill resides in the forecast pre- cipitation fields if they are averaged over area elements of the order of 4° latitude by 4° longitude squares.

Key words: Ensemble forecast; Triangular truncation

1. Introduction

This paper explores an ensemble forecast strategy for the large–scale tropical prediction problem. This is generalized from a recent study on the use of empirical orthogonal function (EOF)–based perturbations for hurricane track ensemble forecasts, (Zhang and Krishnamurti, 1997). In that paper, an ensemble perturbation method was applied for hurri- cane track predictions using the Florida State University's Global Spectral Model at the T63 resolution, which has a horizontal separation of roughly 1.8° latitude / longitude. The wind and temperature fields were perturbed with the order proportional to the respective observational error. It was found that the ensemble prediction method improves the hurricane track forecasts. Our primary interest is in the South China Sea monsoon component where a major international field experiment is presently being carried out by a host of countries in- cluding China, Japan, the United States and Malaysia (Ding et al., 1997; Lau, 1997;

Lau et al., 1998). One of the objectives of this experiment is the predictability of the South China Sea monsoon. The present paper is a preliminary effort in this direction which will again be repeated after the field phase data sets are collected. Divergence of forecasts arising from initial data uncertainties within the framework of ensemble forecasts have not been addressed for the monsoon environment. A goal of this study is to develop initial perturbation techniques for ensemble forecasts for the overall global tropical belt. In this study, we shall make use of a high-resolution global spectral model developed at Florida State University; this is described in Section 2 of this paper. Physical initialization is a major component of our modeling, which permits the inclusion of the initial 'observed rain', based on satellite and surface based observations. The base analysis of our initial state prior to inclusion of perturbations (for the ensemble forecasts) includes physical initialization, which is described in Section 3 of this paper. Ensemble forecasts have become part of operational modeling at various global centers (Toth and Kalnay, 1993; Palmer et al., 1992). They pointed out that optimal perturbations of an ensemble forecast are indeed the fastest growing modes. A number of variations of these ideas have appeared in recent literature. Hoffman and Kalnay (1983) proposed the use of different adjacent start times and thus introduced the notion of lagged average ensemble forecasts. This method allows for the model to select preferred modes while the integration is progressing. Straightforward Monte Carlo method, originally proposed by Leith (1974), for ensemble forecasts, has been persued by several authors, e.g.: Muller and Baumhefner (1994) and by Colucci and Baumhefner (1998). These well known models make use of initializing forecast ensembles at different lead times preceding the onset of an event they studied. The CCM2 version of the Community Climate Model (CCM) of the NCAR was used for this purpose. Our approach differs somewhat from the singular vectors and the breeding methods in that we generate the fastest growing modes from the temporal structure of principal EOF's based on our model runs. This method is described in Section 4 of this paper. The final two sections convey the results and conclusions from this generalized ensemble forecast strategy for the South China Sea monsoon.

2. Global model

The global model used in this study is identical in all respects to that used in Krishnamurti et al. (1991). An outline of the model is as follows:

The model has independent variables $\lambda, \theta, \sigma, t$ (a list of symbols and acronyms appears in Table 1). The dependent variables are vorticity, divergence, temperature and a moisture variable (dew point depression $(T - T_d)$). The model has 384×192 Gaussian transform grid coordinates corresponding to a triangular spectral truncation T-126 in the horizontal. In the vertical, it has 14 layers between 50 hPa and 1000 hPa. Model variables are staggered in the vertical using Charney-Phillips vertical discretization. Vorticity, divergence and geopotential are located at the layer interfaces while temperatures, specific humidity and vertical velocity are assigned at the center of the layers. The vertical grid has higher resolution in the upper troposphere and in the planetary boundary layer. The divergence equation, thermodynamic energy equation and the pressure tendency equation are integrated implicitly while the vorticity and moisture continuity equations are handled explicitly. The tendencies of the physical processes are integrated using a forward time integration scheme. The space differencing scheme utilizes the spectral transform method in the horizontal, centered differences in the vertical are used for all variables except moisture, which is handled by an upstream differencing scheme. The surface topography is based on envelope orography (Wallace et al., 1983).

The model has deep convection based on a modified Kuo cumulus parameterization scheme (Krishnamurti et al., 1983), where moistening and heating parameters are statistically improved over the conventional Kuo-type scheme. The model includes shallow convection (Tiedke, 1984), dry convection and large-scale condensation (Kanamitsu, 1975). We also account for the evaporation of falling precipitation. The surface fluxes of heat, moisture and momentum are calculated using the surface similarity theory (Businger et al., 1971). For low speeds ($\leqslant 5$ ms^{-1}) moisture fluxes are modified following Beljaars and Miller (1990). The vertical distribution of fluxes in the free atmosphere is based on stability (Richardson number) dependent exchange coefficient (Louis, 1979). It also includes a 4th order horizontal diffusion scheme (Kanamitsu et al., 1983). The long and shortwave radiative fluxes are based on a band model that incorporates the radiative effects of water vapor, carbon dioxide, ozone and clouds (Harshvardan and Corsetti, 1989; Lacis and Hansen, 1974). Parameterization of low, medium and high clouds for radiative transfer calculations are based on the definition of threshold relative humidity for three different layers. Fractional areas of various cloud distribution configurations in the vertical are based on a random overlap cloud model. The surface temperatures over the ocean are 10-day averages for the past ten days prior to the start date of the experiment. Over the land, surface energy balance coupled to similarity theory determines the surface temperature including its diurnal cycle (Krishnamurti et al., 1991). Land surface processes are based on Bounoua and Krishnamurti (1993). The initialization of the model is based on physical initialization wherein the moisture field, heat sources and sinks, and divergence fields are initialized consistent with observed OLR and rain rates.

Table 1. List of symbols and acronyms

λ	Longitude
θ	Latitude
σ	Vertical Coordinates ($= p/ps$) where p = pressure and ps = surface pressure
t	Time
P	Observed rain rate
Q_1	Apparent moisture sink
Q_2	Apparent heat source
Q_R	Net radiative heating
T	Temperature
T_d	Dew point temperature
EOF	Empirical Orthogonal Function
CCM	Community Climate Model
NCAR	National Center for Atmospheric Research
NOAA	National Oceanic and Atmospheric Administration
NESDIS-NOAA's	National Environmental Satellite Data and Information Service
UTC	Universal Time Coordinate
DMSP	Defense Meteorological Satellite Program
SSM / I	Special Sensor Microwave Imager
T126	Triangular Truncation 126 Waves
OLR	Outgoing Long Wave Radiation

3. Physical initialization

The physical initialization procedure, developed by Krishnamurti et al. (1991), assimilates the 'observed' rain rates into the atmospheric forecast model. During this process the surface fluxes of moisture, the vertical distribution of humidity, the vertical distribution of mass divergence, the vertical distribution of convective heating, the apparent moisture sink and the surface pressure experience a spin−up consistent with the dynamics and physics for the imposed (observed) rain rates. This is accomplished through a number of reverse physical algorithms within the assimilation mode; these include: a reverse similarity algorithm, a reverse cumulus parameterization algorithm, and an algorithm that restructures the vertical distribution of the humidity variable to provide a match between the model−based outgoing long−wave radiation (OLR) and those based on satellite estimates.

The matching of model calculated OLR with the satellite−based OLR is achieved by modifying the specific humidity above 500 hPa so as to minimize the difference between these two estimates of OLR. This is an important step since the humidity measurements in the upper troposphere from conventional radiosonde are not very reliable. This procedure improves the specification of high and middle clouds and the planetary albedo, resulting in an overall improvement of the model's radiation budget.

The 'observed' rain rates used to initialize rainfall and surface fluxes are obtained through a mix of SSM / I and OLR−derived rain rates and raingauge observations using an algorithm developed by Gairola and Krishnamurti (1992). The SSM / I rainfall is based on the algorithm following Olson et al. (1990).

The reverse similarity algorithm is structured from the vertically integrated equations for the apparent moisture sink (Q_1) and the apparent heat source (Q_2) (Yanai, et al., 1973). Using the observed rain rates, the surface evaporation fluxes are obtained from the sum of the apparent moisture sink (Q_2) and the observed rain rate (P). The surface sensible heat fluxes can be obtained from a knowledge of the apparent heat source (Q_1) and the model−based net radiative heating (Q_R). These surface fluxes of moisture and heat are assimilated by modifying temperature and moisture values within the model's constant flux layer via a reverse similarity algorithm, (Krishnamurti et al., 1991, 1993).

The parameterization of convective precipitation in this model is based on a modified Kuo scheme where major statistical improvements have been incorporated to address the heating, moistening and the rain rate issues (Krishnamurti, et al., 1983). The moisture supply needed for precipitation and moistening is given by vertical convergence of moisture over the convective cloud depth. During physical initialization, the vertical distribution of specific humidity over the convective cloud layers is reanalyzed such that the rainfall implied by the modified moisture convergence in the cumulus parameterization algorithm very closely matches the 'observed' rain rates. The procedure for reconstruction of the moisture variable is based on a reverse cumulus parameterization algorithm detailed in Krishnamurti et al. (1991).

A final step in the physical initialization procedure is a dynamic relaxation within the data assimilation, which, along with the initialization of rainfall and surface fluxes, is applied at each time step during a 24−hour pre−forecast period. This results in a realistic evolution of diabatic heating, moisture and divergence fields, which in turn influences the realistic restructuring of rotational flow and the thermal fields. To ensure that the divergence field evolves rather more freely, consistent with the convective processes, a weaker relaxation coefficient is used for divergence than that for vorticity and surface pressure fields. Table (2) provides a list of these relaxation coefficients.

Table 2. Relaxation coefficients in data assimilation

Vorticity	1.0×10^{-4}
Divergence	0.5×10^{-4}
Surface	Pressure 0.5×10^{-4}
Moisture	Explicit via reverse algorithm
Potential Temperature	0.0

In a recent paper (Krishnamurti et al., 1997) we detail some of the significant capabilities of physical initialization. These include major improvements in the nowcasting of global tropical rainfall; improvements in short range prediction; definition of mesoscale structures of precipitating areas; better definitions of heat sources; better definitions of Hadley and Walker circulations; and improvements in the organization of convection in systems such as hurricanes and monsoons (Krishnamurti et al., 1998).

3.1 *Observed rain rates*

An FSU rainfall algorithm was developed by Gairola and Krishnamurti (1992). Here a mix of rainfall estimates obtained from satellite and surface based observations was used. The satellite component utilizes the brightness temperatures from the DMSP satellites F10, F11, F12 and F13 from its SSM / I instrument to obtain rainfall estimates. The procedure we followed is based on Olson et al. (1990), where the microwave radiances at 19, 22, 36 and 85 GHz are used. These SSM / I data appear along polar orbitor satellite swaths. The footprint of the SSM / I data has average dimensions of the order of 35 km. These SSM / I data are simply collected for 6 hourly data assimilation windows (i.e. ± 3 hours) of the analysis time, and are objectively analyzed using a successive correction scheme. The first guess rainfall for this objective analysis comes from an OLR−based algorithm that was developed by Krishnamurti et al. (1993). This requires 6 hourly fields of OLR. NOAA polar orbitor satellites provide OLR data sets, which are provided on global grids by NOAA / NESDIS. This first guess is obtained by using an OLR−based rain rate algorithm (Krishnamurti et al., 1983). Thus the 'observed' rainfall is kept model independent. Physical initialization assimilates these 6 hourly rain rates. Fig. 1(a,b) presents a comparison of the observed and the initialized rainfall over the global tropical belt for the proposed experiments. Such comparisons usually return a correlation of around 0.9 for the observed versus the initialized rainfall (Krishnamurti et al., 1994). In this illustration we have averaged the four 6−hourly assimilations over a 24−hour period. This type of initialization is fairly robust and has been shown to provide a positive impact for tropical forecasts (Krishnamurti et al., 1993).

4. Ensemble forecasts

This method is called "EOF Based Perturbation Method," (Zhang and Krishnamurti, 1997). Theoretically, the method can be applied to any physical field (wind, geopotential heights, temperature or humidity) over any domain (global or regional). Since the interest of this study lies only in the impact of ensemble prediction on tropical weather systems, we shall only apply this method over the tropics. It is generally agreed that unlike midlatitude disturbances, the wind field is more important than the geopotential height field for large scale flow over the tropics. In order to reduce the computational requirements, only the wind and the

temperature fields were subjected to an EOF analysis. Scaler EOF analysis handles the temperature field, while a complex EOF analysis technique is utilized to handle the wind field, because it permits the depiction of phase changes (Legler, 1983). Furthermore the EOF eigenmodes corresponding to the largest three eigenvalues are used in this study. Finally we add or subtract these three modes to or from the control analysis, in order to obtain a total of seven ensemble members (including the control analysis).

Tropical disturbance growth occurs via a number of instability mechanisms. Nitta and Yanai (1969) have addressed horizontal shear flow instabilities for the growth of equatorial waves in the Pacific Ocean. Moorthi and Arakawa (1985) have pointed out the combined instabilities arising from the effects of vertical shear and convection for the growth of monsoon depressions. The combined barotropic–baroclinic instabilities have been emphasized by Rennick (1976) for the growth of African Waves. Given a high–resolution global model, with
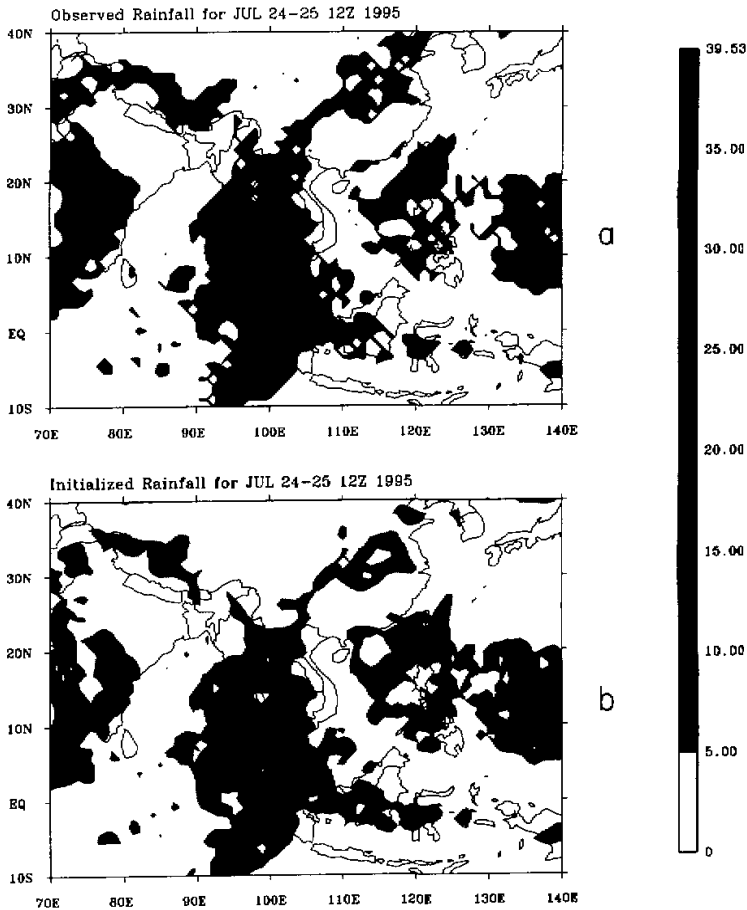

Fig. 1. 24 hourly rainfall total mm / day between July 24 and 25, 1995 12 UTC. a) Estimates based on observations; b) Based on model's physical initialization.

an improved data assimilation component with adequate data coverage and physical initialization, we can expect the nonlinear model itself to sort out the growing modes in a realistic 3-dimensional environment. Our control runs, where the ensemble perturbations are generated, contain the effects of horizontal and vertical shear and of the parameterized (as well as physically initialized) convection; thus we feel that the use of the perturbation growth procedure adopted in our study would be useful in resolving the disturbance growth.

4.1 *EOF-based perturbations*

The perturbation method proposed here recognizes that during the first few days of the model integration (or optimal time) the perturbation would grow linearly. The procedure for this method is to add random perturbations with magnitudes which are comparable to the observational errors of the control analysis. We then integrate the model with its full physics for 36 hours (which we define as an optimal time), starting from the unperturbed (control) as well as the perturbed initial states. These forecast results are stored for every three hours. Upon subtracting the control forecast from the perturbed forecast at corresponding times we obtain the time series of the difference fields at each transform grid point of the model, and we perform an EOF analysis of the time series of the difference fields over the entire tropics. Those modes (eigenvectors), whose EOF coefficients increase rapidly with time, are considered as the fast growing modes, and are used for the definition of the initial perturbations for the ensemble forecasts. An ensemble of initial states is next generated by adding or subtracting these EOF perturbations to or from the control analysis as stated above. This procedure generates a total of 7 perturbed fields where the first two principal components are retained.

5. Results of medium range forecasts

5.1 *Precipitation*

To avoid displaying a large number of illustrations, we shall only show days 3 and 6 of the forecasts. In Fig. 2 (a, b, c, d, e, f, and g) and Fig. 3 (a, b, c, d, e, f and g), we show the results of forecasts for the seven-member ensemble at day three and day six, respectively. Here the rainfall totals are for 24 hours preceding day three in Fig. 2(a through g) and day six in Fig. 3(a through g). Figs. 2h and 3h illustrate the observed rainfall on day three and day six, respectively. The individual members show considerable variability over the South China Sea. The outer shading denotes rainfall totals of the order of 10 to 20 mm / day. The heavy rain areas to the north of the Philippines arise from Tropical Storm Gary where the maximum rainfall amounts are in excess of 100 mm / day. Most ensemble members show a similar distribution and intensity of rainfall over northern India. Panel e differs in this regard from most other panels. In general, the predicted precipitation amounts near and to the east of the storm center were larger than the observed estimates (panels a, c, d, e, f, g).

By day six, we still note a skill in the details of precipitation forecasts. The 24-hourly observed precipitation between days five and six (superimposed on those flow patterns) shows heavy rain west of the Philippines, a feature that was captured by several ensemble members (panels a, c, d, and e). The near equatorial rainfall is reasonably handled by ensemble members b, c, and d. Most models show somewhat excessive rainfall during this period over the Asian continent along 20°N. Panel e shows closer agreement to the observed rains displayed in panel h.
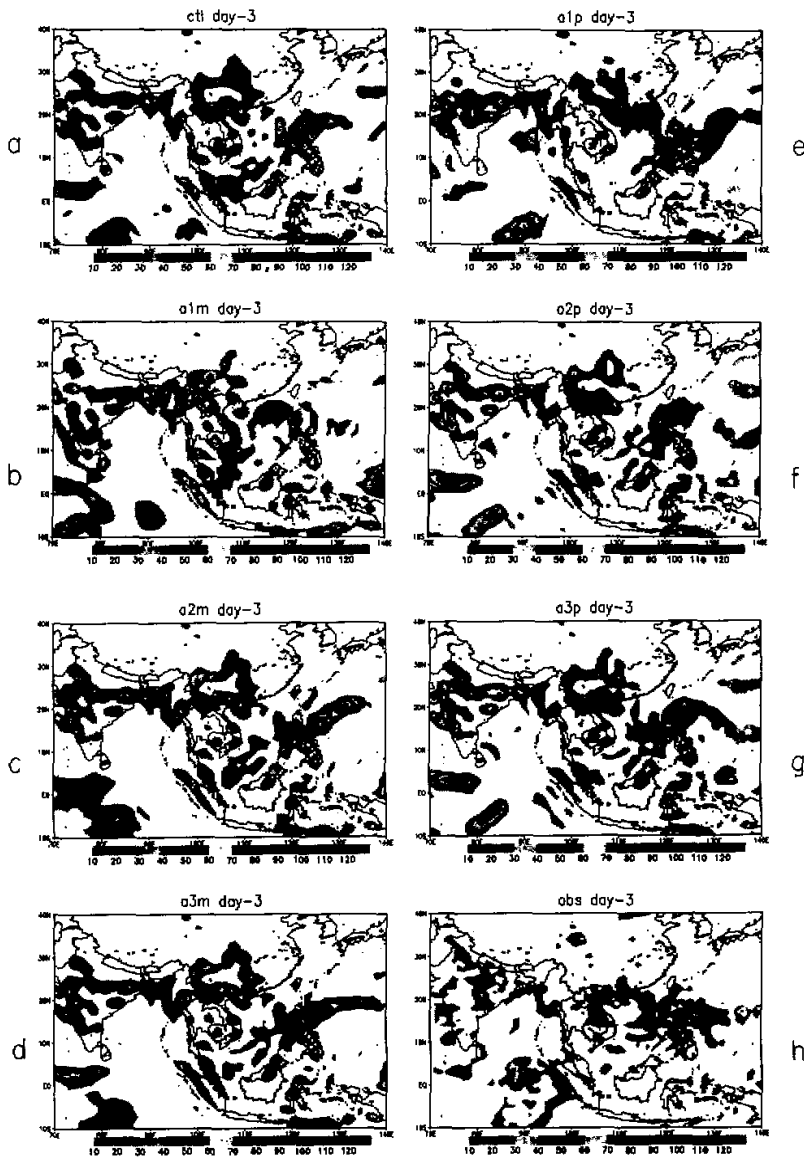
Fig. 2. Panels a through g show the forecasts of rain between days 2 and 3 forecast for the 7 ensemble members; units mm / day. Panel h shows the estimates of rain based on observations for this period, i.e. July 27 to July 28, 1995 12 UTC.
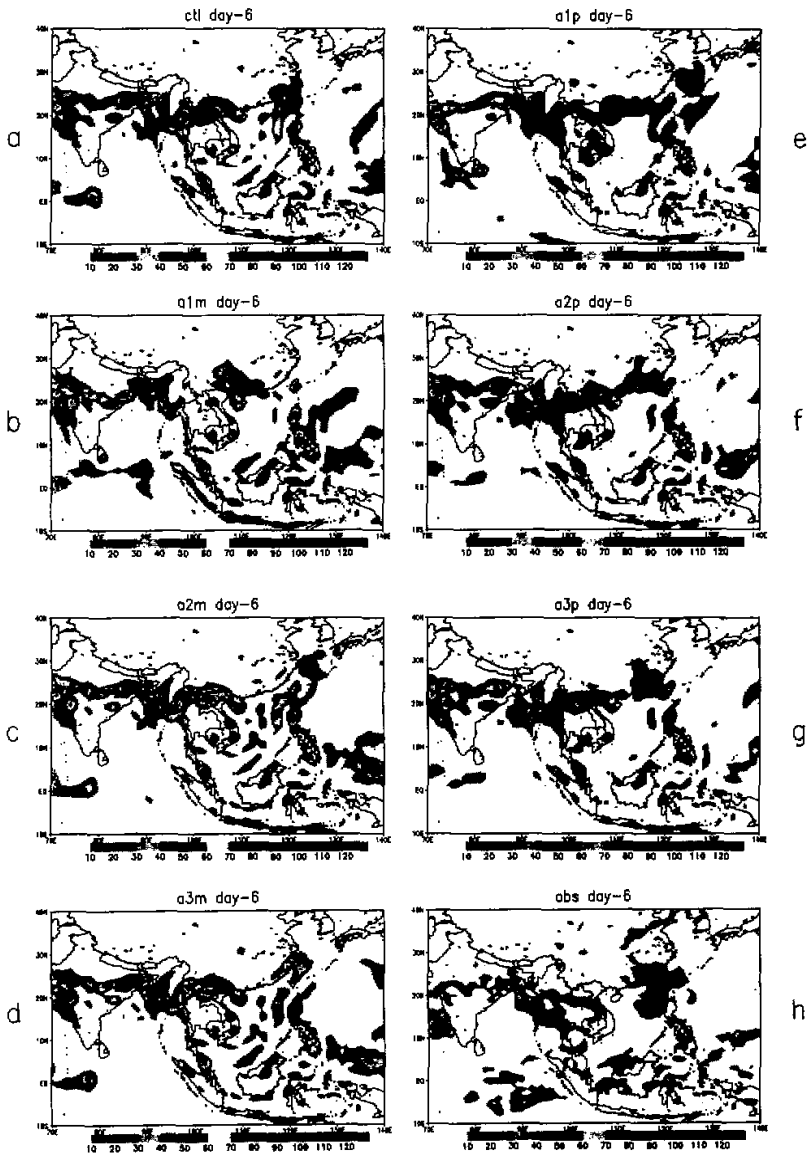
Fig. 3. Same as Fig. 2 but for day 5 to day 6 of ensemble forecast, i.e. July 30 to July 31, 1995 12 UTC.

5.2 850 hPa winds

In Fig. 4(a,b, ⋯ h) we show the streamlines and isotachs at day three of the forecast for the seven-member ensemble. The observed flow field over the South China Sea was quite zonal. The predicted flow fields in panels c, d, e, and g showed such zonality. The observed field contains a prominent axis of anticyclonic flows that extends from southwest to northeast over the South China Sea. That sort of feature is indeed present in several of the ensemble member forecasts. Some of the forecasts captured this feature better (panels c and e) than others (panel b). The monsoonal southwesterly flow (in the observed field) exhibits a weak trough to the east of the Indochina peninsula over the South China Sea. That feature was also captured in several forecasts (panels c, d, g). The wind speed at 850 hPa was quite reasonably predicted at day three of forecasts by several ensemble members (Fig. 4). The predicted wind speed shown in panels a, f, and g bears a strong resemblance to the observed field shown in panel h. On day three, the observed storm (Gary) was located over the northern Philippines. Predicted position of this storm was located $10°$ longitude to the west for member b and as much as $20°$ longitude to the east for member d. Most other members of the ensemble located the storm close to the northern part of the Philippines. The location of the strongest lower tropospheric winds located to the east of Tropical Storm Gary is not reasonably predicted with respect to its center by any of the ensemble members. The South China Sea monsoon (in the analysis field—based on observations, panel h) is distinctively portrayed as the trade wind easterlies south of the equator, which acquire cross-equatorial southerly flow near the equator and a southwesterly monsoonal signature over the South China Sea. This classical pattern of the South China Sea monsoon is not described fully by any of the ensemble members, however as we shall show in Section 5d, the ensemble average of the forecasts on day three does seem to describe these features much better than the individual ensemble members. The ensemble forecasts at day six for 850 hPa are shown in Fig. 5(a through g) and the analysis fields based on observations are shown in Fig. 5(h). The salient observed feature in the flow field is an extended ridge which is connected from southwest to northeast along the entire length of the South China Sea. Such a feature is captured by most members of the ensemble, although the orientation of that axis is not entirely southwest to northeast in many cases. Some of the better forecasts are seen in panels d, f, and g. The wind speed in the southwest monsoon, north of this ridge, lies between 10 to 20 ms^{-1}. Panels e, f, and g show this feature very clearly. A local intense wind maxima, >20 ms^{-1}, to the west of Korea is not seen in any of the ensemble forecasts. A wave in the equatorial easterlies, near $120°E$, moved somewhat slowly westward in the six-day forecasts and can be seen only in panels b and d where it was located close to $130°E$. In general these broad easterlies were reasonably predicted by all members of the ensemble. The continental monsoon trough along $20°N$, west of $110°E$, was reasonably predicted by several members of the ensemble (panels a, c, d, f, and g); overall this six-day ensemble forecast contained important ingredients for ensemble averaging.

5.3 200 hPa winds

The observed and ensemble member forecasts of the 200 hPa wind field, for day three, are shown in Fig. 6(a through h). Panel h shows the observed winds. The other panels are the ensemble member forecasts for day three. We notice a clear easterly bias in the forecasts of the tropical easterly jet near $7°N$. Most ensemble members show winds in excess of 30 ms^{-1},
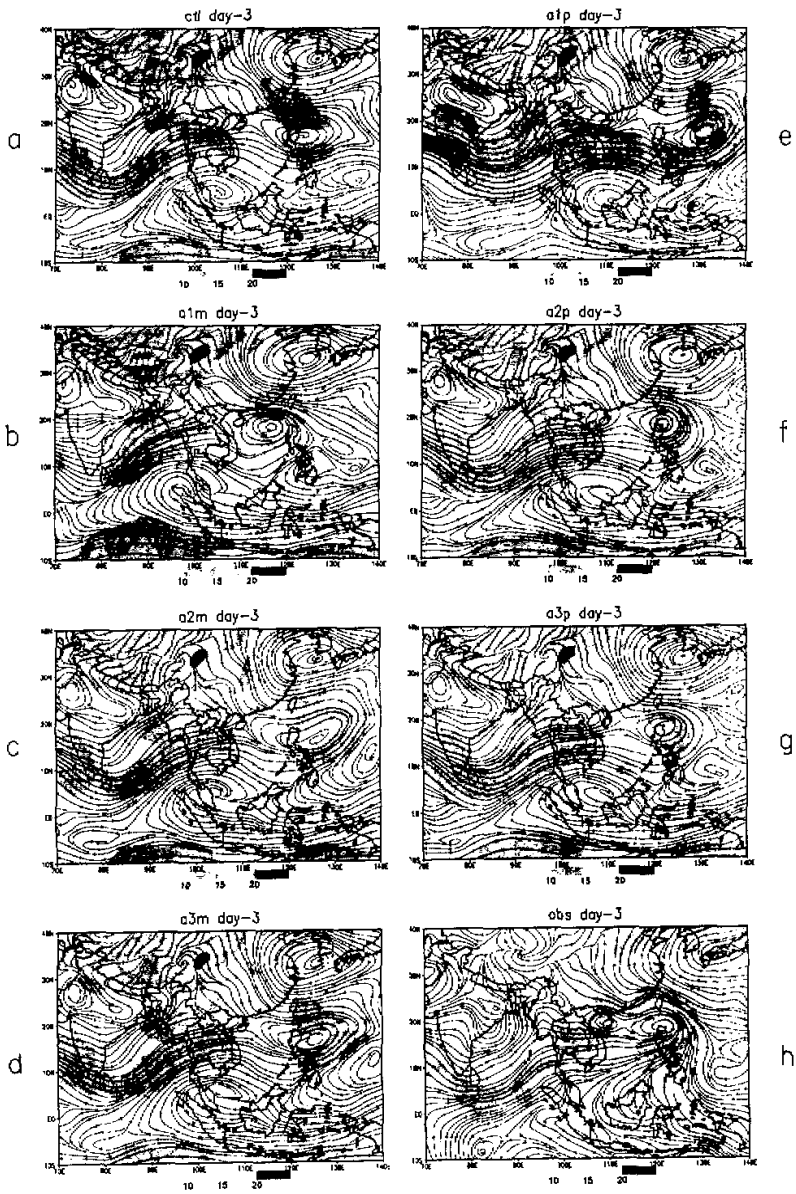
Fig. 4. Streamlines (solid lines) and isotachs (shaded) ms^{-1} at 850 hPa. Panels a through g show the results of ensemble forecasts for day 3 of forecast. Panel h shows the field based on observations for day 3, i.e. July 28, 1995 12 UTC.
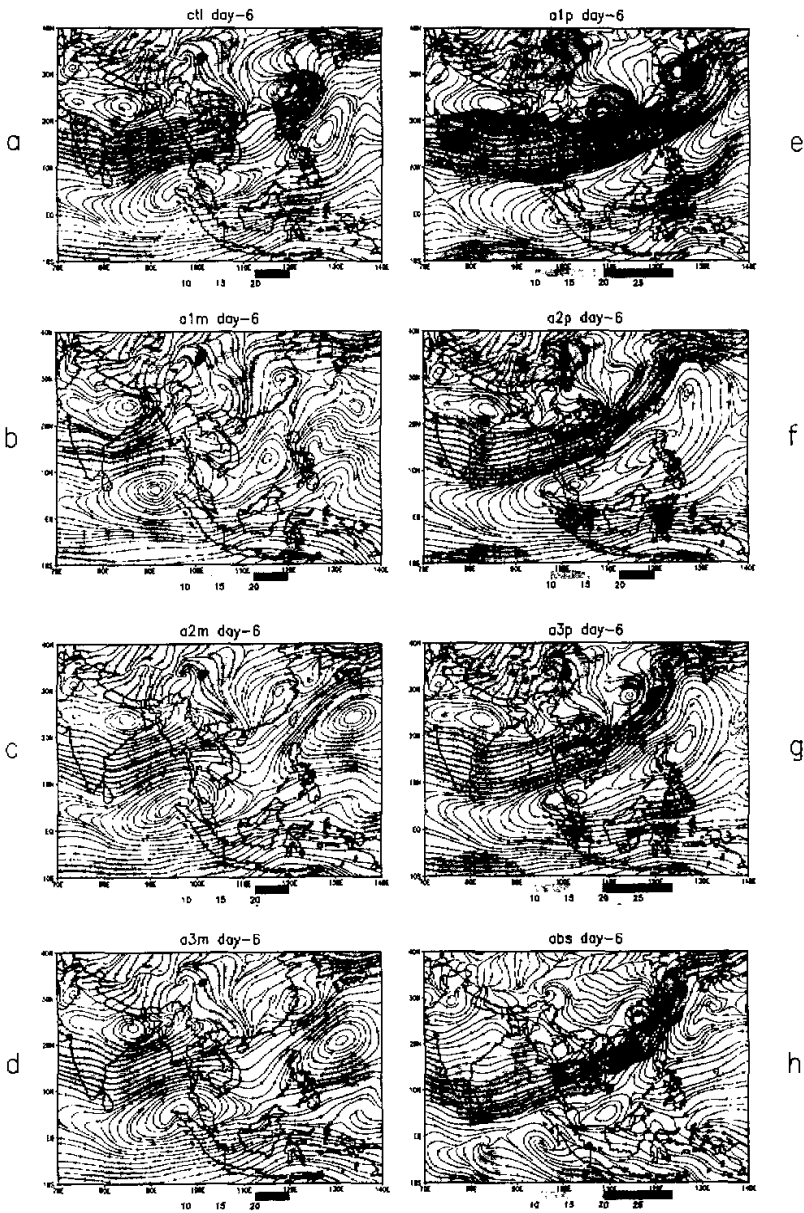
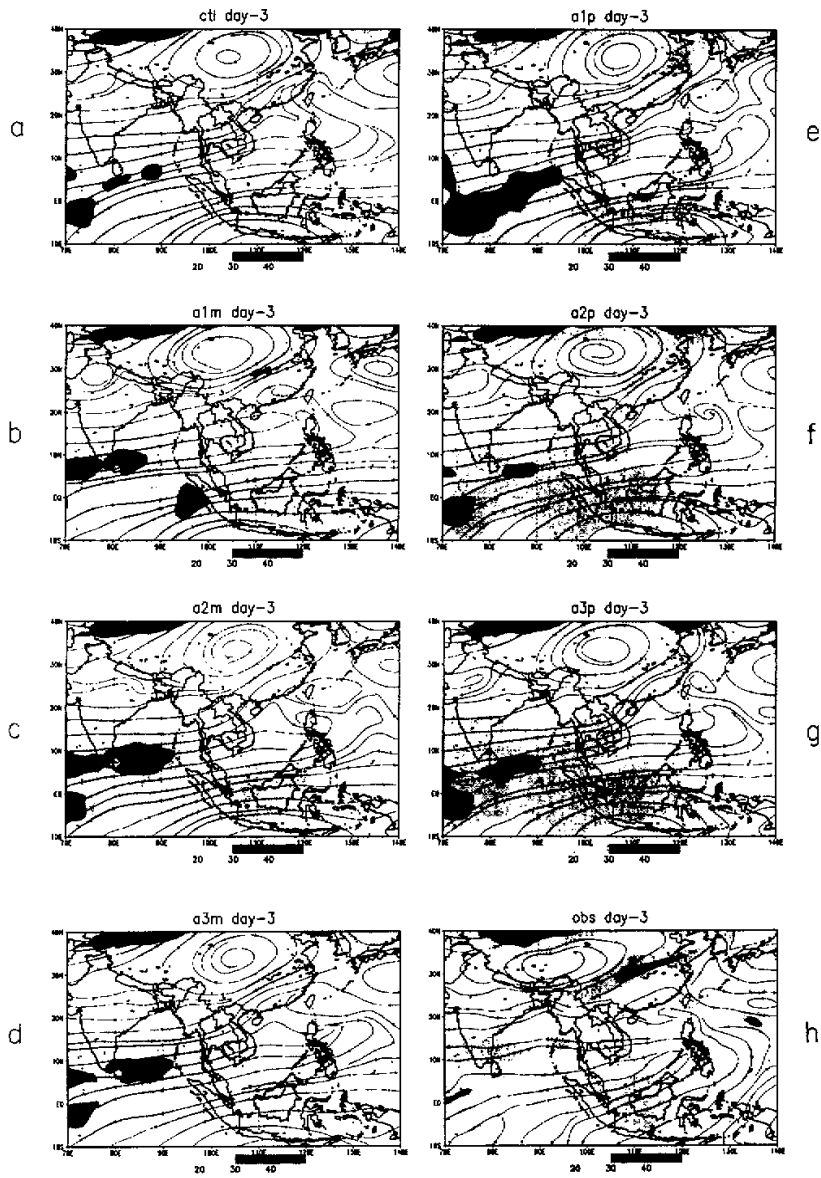Fig. 5. Same as Fig. 4 but for day 6 of forecasts, i.e. July 31, 1995 12 UTC.

Fig. 6. Same as Fig. 4 but for 200 hPa level for day 3 of forecasts.

whereas the analysis shows weaker winds. The entire bias may be a reflection of sparse data that leads to an underestimate of the observed jet. These fields for day-6 are shown in Fig. 7 (a through h). The model and the observations show a belt of strong easterlies (20 to 30 ms^{-1}) between 5°S and 15°N. A striking feature, strong northeasterlies in excess of 30 ms^{-1} over Borneo, in the observed field is not captured at day-6 of the forecast. We do see some strong winds of this intensity over the South China Sea in some of the ensemble member forecasts. Northeasterly winds over Borneo are of the order of 20 to 30 ms^{-1}, and these are reasonably handled by most ensemble members. The center of the Tibetan anticyclone is located near 95°E and 30°N. The latitudinal location is very well predicted by most ensemble members, however we note a somewhat eastward shift in its location in the forecasts. This may also be related to sparse upper air data over the region.

5.4 *Ensemble averages*

The ensemble averaged forecast sequence for the 6-day forecast is shown in Fig. 8(a through f). The corresponding observed flow fields are shown in Fig. 9(a through f). Here the 850 hPa winds (streamlines and isotachs) from July 26, 1995, 12 UTC to July 31, 1995, 12 UTC are shown. These are based on the averages of the physically initialized seven forecast fields of the ensemble members. Day-1 of the forecast predicts the anticyclone over the southern part of the South China Sea, Tropical Storm Gary east of the Philippines, the monsoon trough over the northern Bay of Bengal, a monsoon depression over the Pakistan / India border and a major anticyclone over Japan. Overall, all major circulation features are reasonably predicted. Forecasts on day-2 also show a remarkable skill in predicting all major circulation features. Except for a weakening of the Bay of Bengal disturbance over northeastern India, most circulation features are quite reasonably handled by the ensemble mean of the forecasts at day-3. The forecasts on day-4 show a remarkable skill in handling the strength of westerly monsoon flow between 10° and 20°N, the position of Tropical Storm Gary and the monsoon depression over central India.

The latitude of a near-equator buffer zone is positioned somewhat too far north in the ensemble mean forecasts on day-4. That contributes to a weaker prediction of the cross-equatorial monsoon flow. The strength and latitudinal extent of the westerly monsoon flow from India to the Pacific coast of Vietnam are very well predicted in days 5 and 6 of the ensemble mean forecasts. Tropical Storm Gary weakens in the forecasts by days 5 and 6. The tropical storm forecasts on days 5 and 6 were handled reasonably by only 2 of the 7 members. In a straight ensemble averaging this tends to weaken the circulation. Overall the ensemble averaged forecasts appear to hold skill in describing the circulation features through day-4 of forecasts. The forecasts over the Tibetan Plateau need to be discounted for the 850 hPa surface since the analysis portrays extrapolations from a sigma coordinate surface to an 850 hPa surface where the surface elevation is well above 850 hPa.

5.5 *Sea level pressure forecasts over the South China Sea*

Ensemble forecasts for days 3 and 6 of the sea level pressure (hPa) are shown in Fig. 10 and Fig. 11, respectively. Here the bottom right panel shows the fields based on 'observations' and the remaining depict the ensemble forecasts. On day-3, Tropical Storm Gary was located over the northern tip of the Philippines. The locations of minimum surface pressure for this storm, for ensemble members f and g, provide reasonable forecasts. Several members show a slower westward motion (such as c, d, and e), whereas member b shows too fast a westward
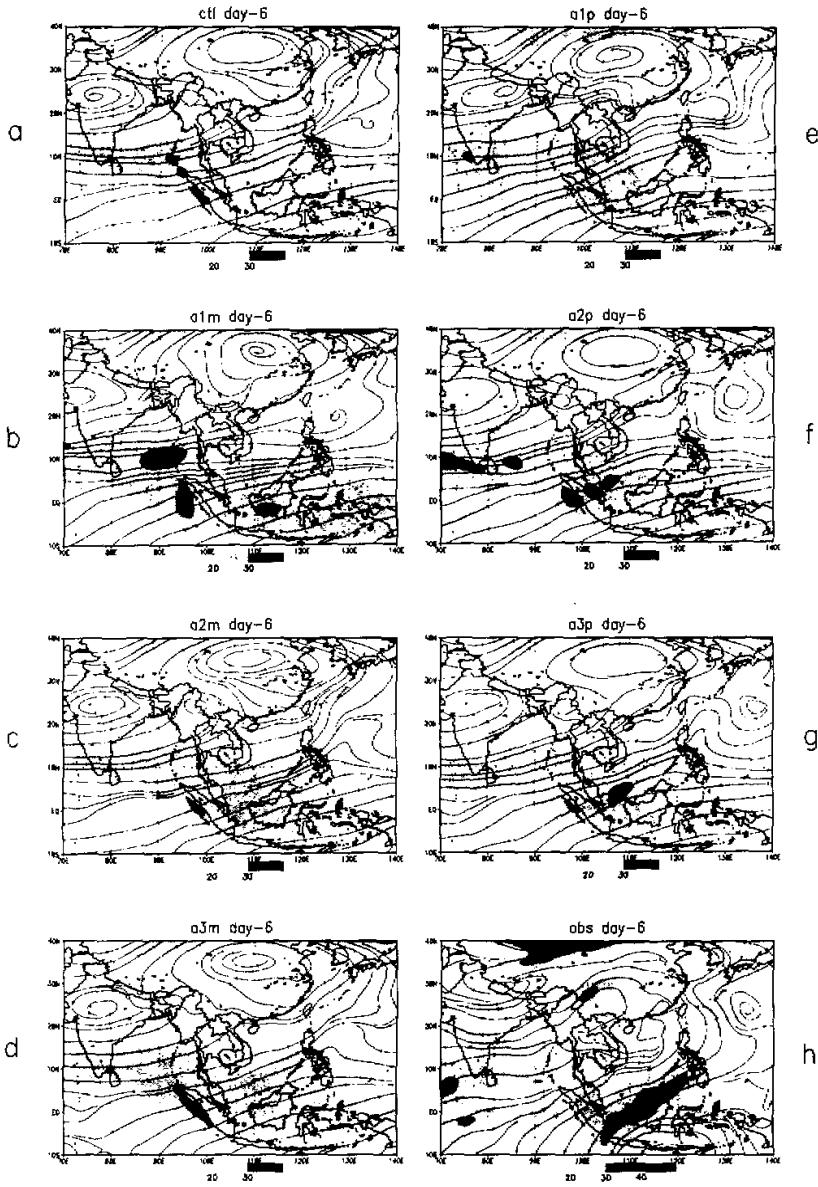
Fig. 7. Same as Fig. 5 but for 200 hPa level for day 3 of forecasts.

motion. Over the South China Sea the observed pressure field shows a weak monsoon trough along 20°N. That feature was captured by most ensemble members. To the south of the equator near 110°E, pressures higher than 1010 hPa were observed; that was also carried by most ensemble forecasts. By day−6, the tropical storm had made landfall in China. Most ensemble members weaken this storm prior to day−6; thus a distinct signature of the low pressure (just below 1000 hPa) is not noted. The storm is distinctly seen only in ensemble member forecasts for panels e and g. Panel g shows a somewhat faster northerly track. The subtropical high located near 30°N and 130°E is an important feature. Over the northern part of the South China Sea the isobars are aligned south to north (an east−west pressure gradient). The day−6 forecasts show this feature for all of the ensemble members (a, b, c, d, e, f and g). To the south (around 10°S), pressure as large as 1010 hPa (or somewhat higher) is also reflected in most

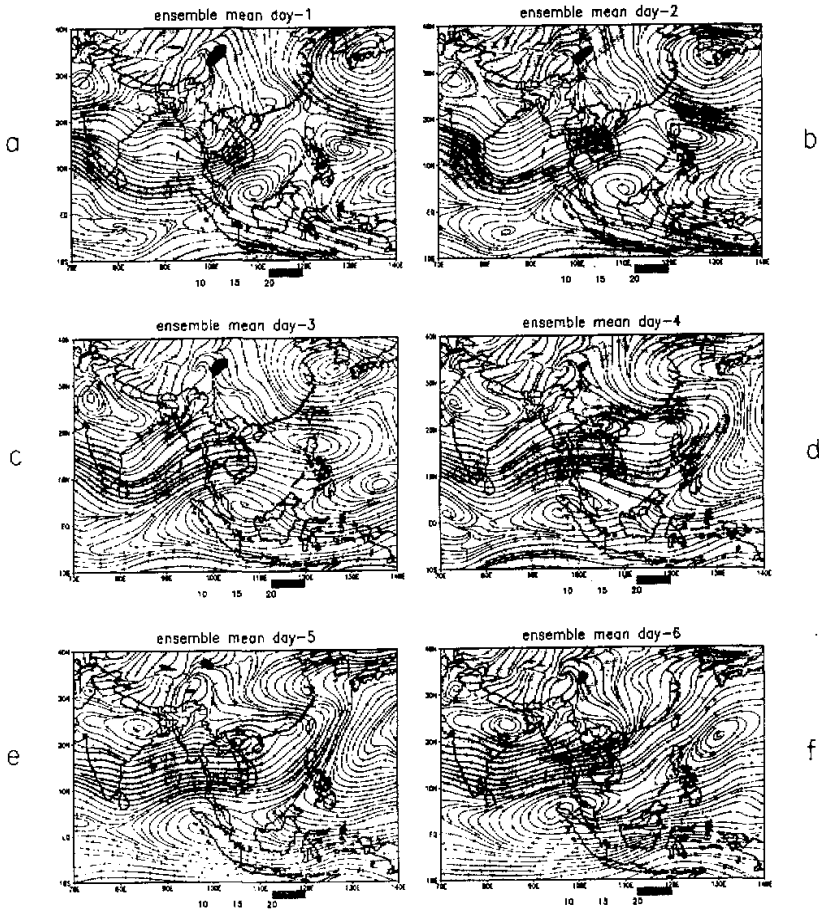

Fig. 8. Ensemble averaged forecasts between day 1 through day 6 (July 26 to July 31, 1995 12 UTC). Streamlines (solid lines) and isotachs (shaded) ms^{-1} at 850 hPa.

obs day—1   obs day—2

a   b

10   15   10   15

obs day—3   obs day—4

c   d

10   15   20   10   15   20

obs day—5   obs day—6

e   f
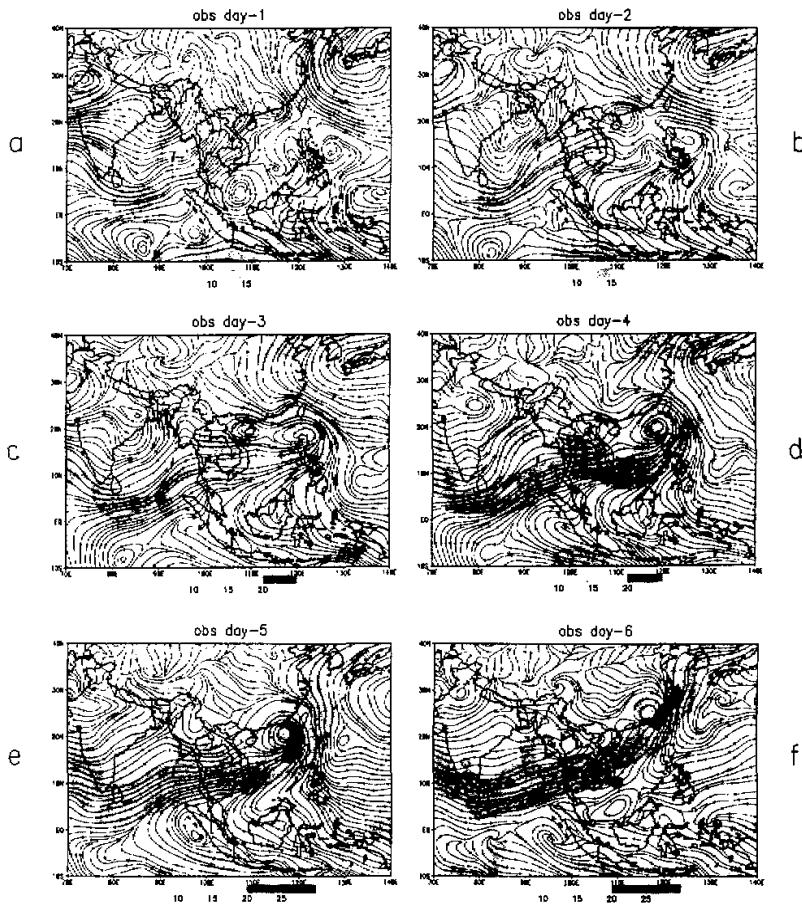
10   15   20   25   10   15   20   25

Fig. 9. Observed fields of 850 hPa streamlines (solid lines) and isotach (shaded) ms^{-1} between days
1 through 6, i.e. July 26 to July 31, 1995 12UTC.

ensemble member forecasts. Overall, the 6-day forecasts over and around the South China
Sea appear quite reasonable.

5.6 RMS errors of ensemble forecast

Here we shall compare the root mean square (rms) errors of an ensemble averaged fore-
cast with that of the first run which was the control experiment. All experiments were carried
out over the global domain at resolution T-126 (which has an approximate transform grid
separation of 60 km over the South China Sea). The results over a sub-domain of the South
China Sea enclosing 10°N to 40°N and 70°E to 140°E are presented in Fig. 12. The top panel
shows the results for 850 hPa for this sub-domain and the bottom panel covers the results for
the global tropical belt 25°S to 25°N. The solid lines are the rms errors (units: ms^{-1}) for the
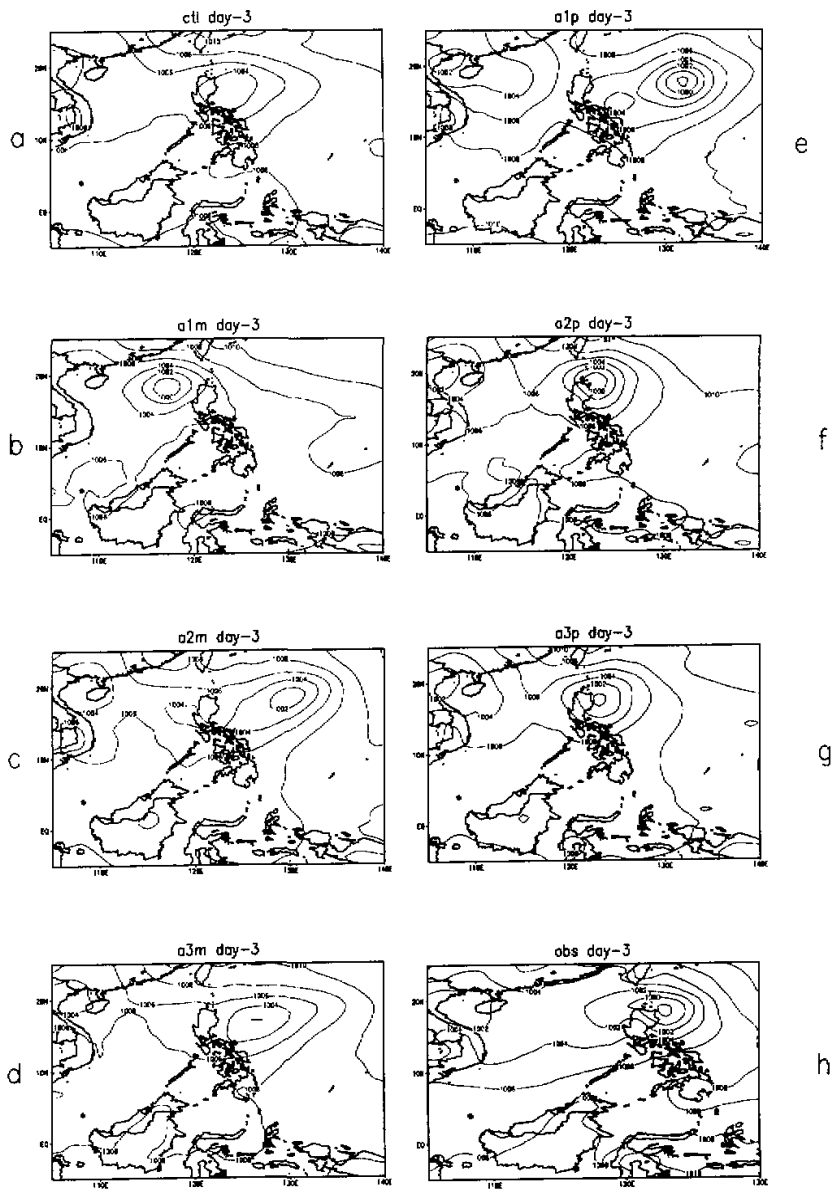
Fig. 10. Sea level pressure, hPa, for the seven member ensemble forecasts are shown in panels a through g for day 3 (July 28, 1995 12UTC) of forecast. Panel h shows the corresponding observed field.
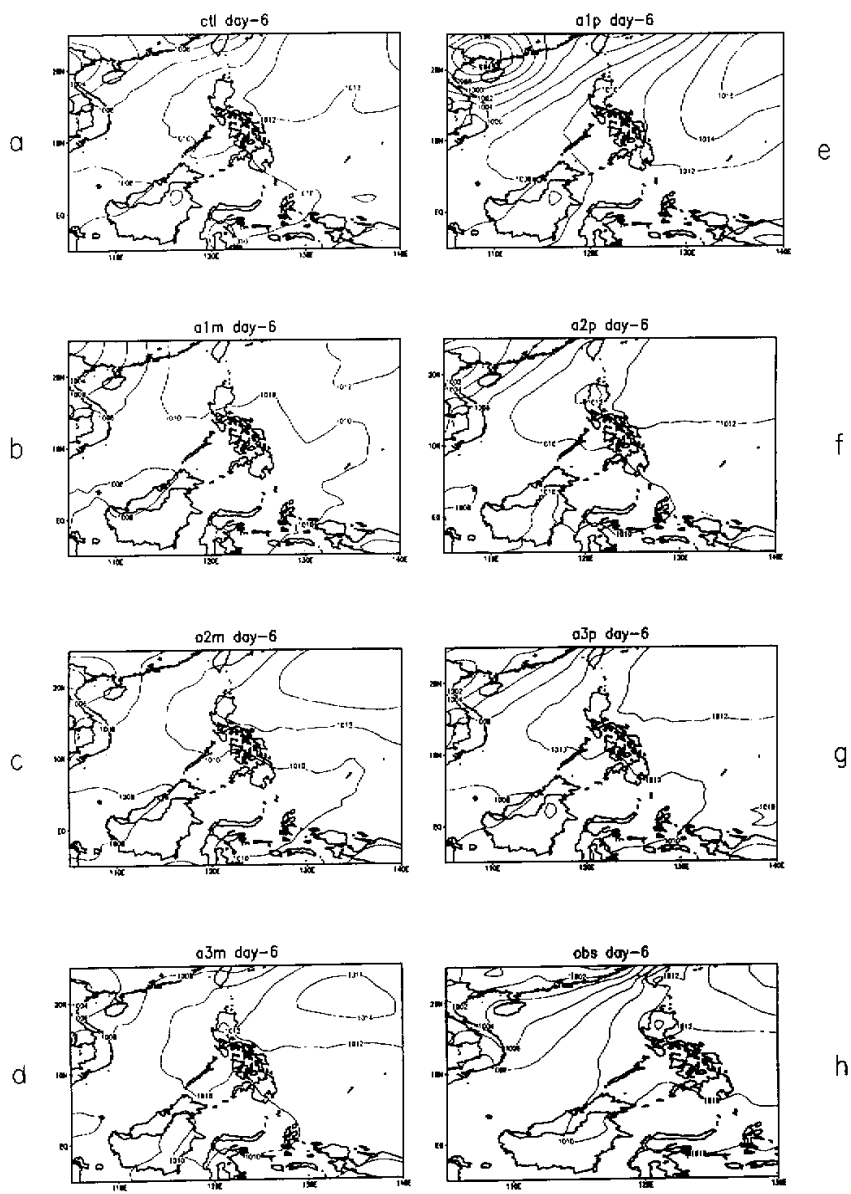
Fig. 11. Same as Fig. 10, but for day 6 (July 31, 1995 12 UTC).
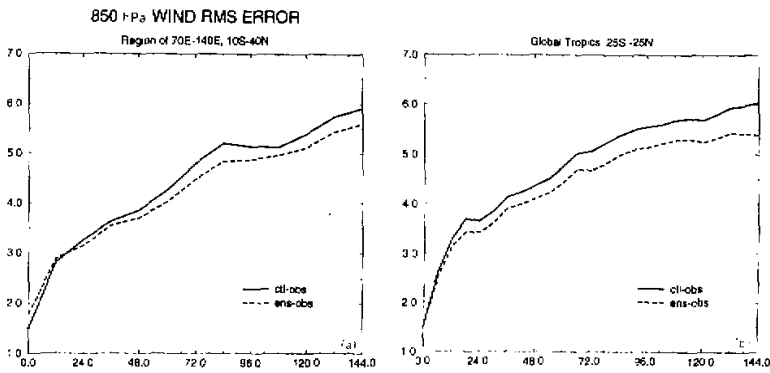
850 hPa WIND RMS ERROR

Fig. 12. Root mean square error of the wind forecasts at 850 hPa for a) South China Sea monsoon domain; b) global tropical domain between 25°S to 25°N. Solid line shows the results for the ensemble average of the forecasts and the dashed lines show the results for the control experiment.

control experiment and the shaded lines are for the ensemble averaged forecast. Here we present the results from averaging the wind forecasts from all 7 ensemble members over a 6-day forecast period. The ensemble averaged forecast performs better than the control, both regionally and globally. This is a promising result for tropical numerical weather prediction.

5.7 Ensemble mean precipitation

We have noted a marked skill in rainfall forecasts, if one takes into account the phase errors that arise from the motion of precipitating systems. We shall first show correlations of observed and predicted rainfall over the South China Sea monsoon domain for the different members of the ensemble and for the ensemble averaged forecast. Fig. 13 illustrates histograms of correlation for the ensemble members and the ensemble mean. Results for days 0, 3 and 6 of forecasts are shown for each panel. Within these illustrations the vertical barbs are for different horizontal area averages (prior to the evaluation of correlations) for the forecast and the observed rain. The lightly shaded vertical bars denote an averaging of the precipitation over 1° squares, the dark shading denotes averaging over 2° squares and the unshaded vertical bar denotes averaging over 4° squares. Such averaging shows an improved skill if the averaging areas confine the major precipitating systems, thus reducing the rms error arising from phase errors. The main results from this illustration are that rainfall skill is still quite large, even for day 6 of forecast over the South China Sea domain, if an averaging is extended over elementary areas of 4° latitude by 4° longitude prior to the calculation of rms skill. That correlation is of the order of 0.4. If no averaging is performed (i.e. model rainfall at the 1° lat / lon resolution of the model), the correlation at day-6 is of the order of 0.25 to 0.30. The averaging improves the correlation skill by taking into account the phase errors. The ensemble mean has a higher skill compared to some members, such as those for members c and e, but is not conspicuously better than most other members. Overall we are able to extend the prediction skill through day-6 of a forecast by this averaging. The geographical distribution of the predicted ensemble mean rain and the observed estimates for days 3 and 6 of
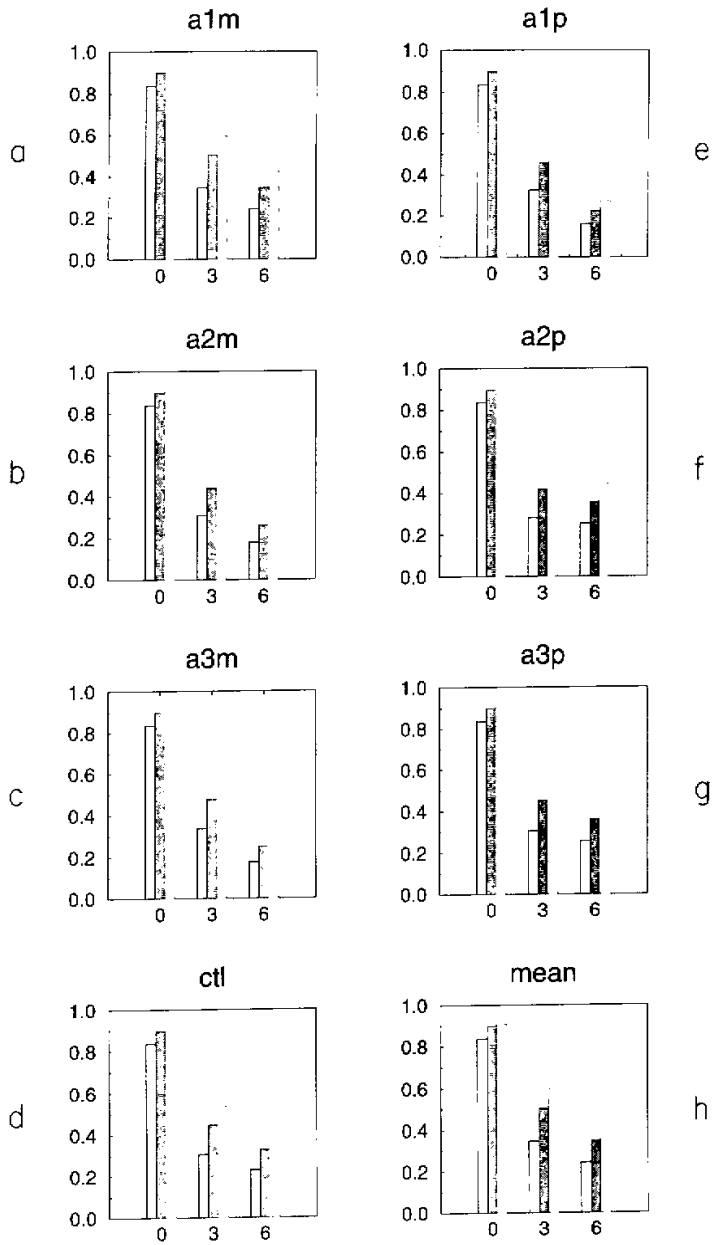
Fig. 13. Precipitation forecast correlation for the 7 ensemble members shown in panels a through g and panel h shows the results for the ensemble mean. Each illustration includes the correlation for days 0, 3 and 6; where the light shaded barb denotes results based on precipitation averaged over 1° squares prior to the computation of the correlation. The dark shading and the open barbs denote similar averaging over 2° and 4° squares respectively.
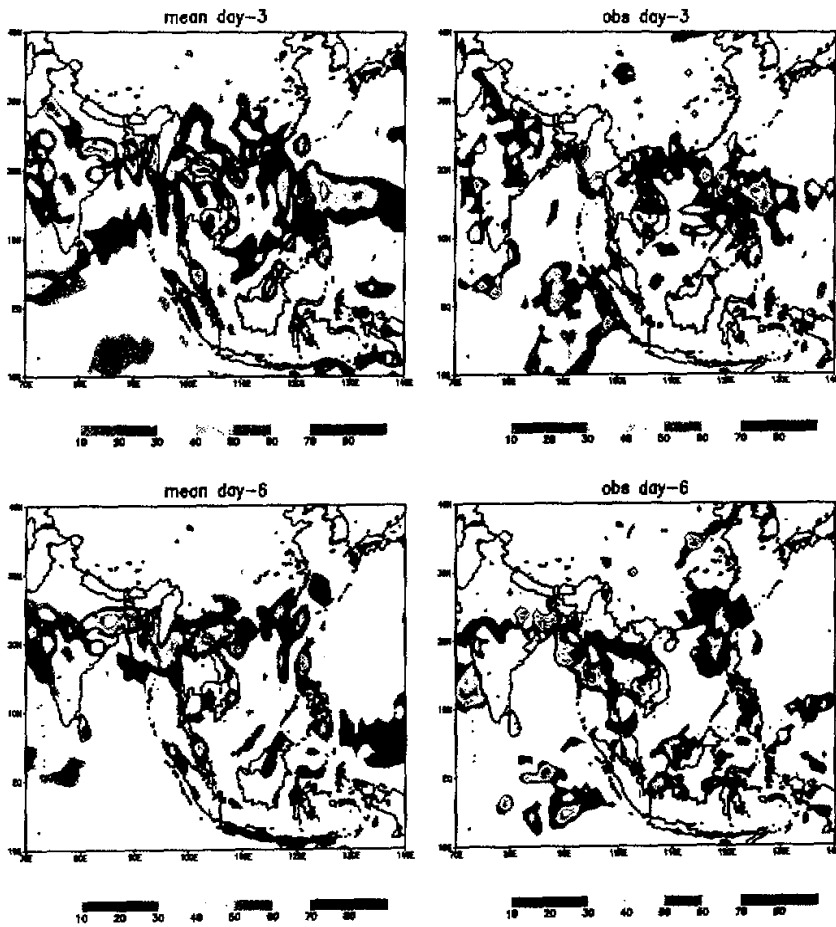
Fig. 14. Comparison of ensemble averaged predicted precipitation (mm / day) against observed es-
timates for days 3 and 6 of forecasts. a) day 3 ensemble forecast; b) observed measures for day 3; c)
day 6 ensemble forecast; and d) observed measures for day 6.

forecasts are shown in Fig. 14 (a, b, c and d). The activity of rainfall over central India, north-
ern Bay of Bengal and the northern part of the South China Sea (arising from Tropical Storm
Gary) is reasonably handled through day-6 of the forecast. At day-3 we are looking at fields
that have a correlation of around 0.35 and at day-6 around 0.3. The information content
calls for higher correlation if these fields were averaged over, for example, 4° latitude / longi-
tude squares. Several members of the ensemble contribute to excess rain over India for both
days 3 and 6, whereas a few members have rainfall amounts comparable to observations. The
excess rainfall over India in Fig. 14 arises from data uncertainties and the sensitivity of fore-
casts to initial perturbations. The choice of a 7-member ensemble may not be adequate since

this choice might have placed a bias on the large excess of rain producing initial perturbations.

6. Conclusions and future work

This study makes use of EOF-based perturbations to carry out global forecasts. A seven-member ensemble utilizes the first three EOFs of growing modes, where the initial winds and the temperature fields were perturbed globally. The amplitudes of these initial perturbations were comparable to the typical observational errors in the temperature and wind measurements, i.e. of the order of $\pm$ 1°C and 1 ms^{-1}, respectively. The rms wind and precipitation errors clearly show that the ensemble average has a higher skill compared to the control experiment. All of these experiments invoked physical initialization (inclusion of observed rain in the data assimilation). That led to a large reduction of the ensemble spread, which may have been an undesirable aspect of this study. Large perturbations in the initial states can provide a very large spread for ensemble forecasts (in the absence of physical initialization); that too can be undesirable. What is perhaps needed is a reasonable spread of forecasts; we do not have a design of such an experiment at the present time. Physical initialization retains the rotational parts of the winds; however the divergent parts of the wind, the moisture and the initial heating fields are very close for all experiments since the same observed rainfall rates are assimilated. This tends to reduce the spread of ensemble forecasts (Krishnamurti et al., 1997). The present study does show an improvement of forecast skill through day-6 of forecasts arising from the use of EOF-based perturbations, physical initialization and ensemble averaging. Further work is needed to address the issues of forecast spreads where various parameters such as the number of EOF modes, resolution and a better use of physical initialization are examined in detail.

REFERENCES

Beljaars, A., and M. Miller, 1990: A note concerning the evaporation from the tropical oceans: sensitivity of the ECMWF model to the transfer coefficient of moisture at low wind speed. ECMWF Research Department Technical Memo 170, ECMWF, Reading, 19 pp.

Bounoa, L., and T.N. Krishnamurti, 1993: Influence of soil moisture on the Sahelian Climate Prediction I. *Meteor. Atmos. Phys.*, **52**, 183-203.

Businger, J.A., et al., 1971: Flux profile relationship in the atmospheric surface layer. *J. Atmos. Sci.*, **28**, 181-189.

Colucci, S.J., and D.P. Baumhefner, 1998: Numerical Prediction of the Onset of Blocking: A case study with forecast ensembles. *Mon. Wea. Rev.*, **126**, 773-784.

Ding, Y., et al., 1997: The South China Sea Monsoon Experiment (SCSMEX) Implementation Plan. *Advances in Atmospheric Sciences*, **14**, 255-270.

Gairola, R.M., and T.N. Krishnamurti, 1992: Rain rates based on SSM/I, OLR and raingauge data sets. *J. Meteor. Atmos. Phys.*, **50**, 165-174.

Harshvardan, and T.G. Corsetti, 1984: Longwave parameterization for the UCLA/GLAS GCM. NASA Tech. Memo 86072, Goddard Space Flight Center, Greenbelt, MD.

Hoffman, R.N., and E. Kalnay, 1983: Lagged average forecasting, an alternative to Monte Carlo forecasting. *Tellus*, **35A**, 100-118.

Kanamitsu, M., et al., 1983: Description of the JMA operational spectral model. *J. Meteor. Soc. Japan*, **61**, 812-828.

Kanamitsu, M., 1975: On numerical weather prediction over a tropical belt. Report No. 75-1, Dept. of Meteorology, Florida State University, Tallahassee, FL 32306, pp. 1-282.

Krishnamurti, T.N., et al., 1998: Organization of Convection and Monsoon Forecasts. Meteorology and Atmospheric Physics Riehl Special Volume (in press).

Krishnamurti, T.N., et al., 1997: Physical Initialization and Hurricane Ensemble Forecast. *Weather and Forecasting*, **12**, 503–514.

Krishnamurti, T.N. et al., 1997: Physical Initialization. *Atmosphere–Ocean*, **35**, 369–398.

Krishnamurti T.N. and H.S. Bedi, 1996: A brief review of Physical Initialization. *Met. Atmos. Physics*, **60**, 137–142.

Krishnamurti, T.N., et al., 1993: Physical Initialization using the SSM / I Rain Rates. *Tellus*, **45A**, 247–269.

Krishnamurti, T.N., et al., 1991: Physical initialization for numerical weather prediction over the tropics. *Tellus*, **43AB**, 53–81.

Krishnamurti, T.N. and H.S. Bedi, 1988: Cumulus parameterization and rainfall rates: Part III. *Mon. Wea. Rev.*, **116**, 583–589.

Krishnamurti, T.N., et al., 1983: Cumulus parameterization and rainfall rates, Part II. *Mon. Wea. Rev.*, **111**, 815–828.

Kuo, H.L., 1974: Further studies of the parameterization of the influence of cumulus convection on large scale flow. *J. Atmos. Sci.*, **31**, 1232–1240.

Lacis, A.A. and J.E. Hansen, 1974: A parameterization of the absorption of solar radiation in the earth's atmosphere. *J. Atmos. Sci.*, **31**, 118–133.

Lau, K.-M. et al., 1998: Hydrological processes associated with the first transition of the Asian summer monsoon a pilot satellite study. *Bull. Am. Meteor. Soc.* (in press, September issue).

Lau, K.-M., 1997: South China Sea Monsoon experiment observed from satellites. *EOS Transactions, AGU*, **78**, 599–603.

Legler, D.M., 1983: Empirical orthogonal function analysis of wind vectors over the tropical Pacific Region. *Bull. Amer. Meteor. Soc.*, **64**, 234–241.

Leith, C.E., 1974: Theoretical skill of Monte Carlo forecasts. *Mon. Wea. Rev.*, **102**, 409–418.

Louis, J.F., 1979: A parametric model of vertical eddy fluxes in the atmosphere. *Boundary Layer Meteorology*, **17**, 187–202.

Moorthi, S. and A. Arakawa, 1985: Baroclinic Instability with Cumulus Heating. *Mon. Wea. Rev.*, **42**, 2007–2031.

Mullen, S.L. and D.P. Baumhefner, 1994: Monte Carlo simulations of explosive cyclogenesis. *Mon. Wea. Rev.*, **122**, 1548–1567.

Nitta, T. and M. Yanai, 1969: A note on the barotropical instability of the tropical easterly current. *J. Meteor. Soc. Japan*, **47**, 127–130.

Olson, W.S., et al., 1990: Recommended algorithms for the retrieval of rainfall rates in the tropics using SSM / I (DMSP–F8). Manuscript, University of Wisconsin, Madison, 10pp.

Palmer, T.N., et al., 1992: Ensemble prediction, ECMWF Tech. Memo, 188 [Available from ECMWF, Shinfield Park, Reading RG29AX, United Kingdom].

Tiedke, M., 1984: The sensitivity of the time–mean large–scale flow to cumulus convection in the ECMWF model. Workshop on Convection in large–scale numerical models. ECMWF, 28 Nov. – 1 Dec. 1983, 297–316.

Toth, Z. and E. Kalney, 1993: Ensemble forecasting at NMC. The generation of perturbations. *Bull. Amer. Meteor. Soc.*, **74**, 2317–2330.

Wallace, J.M., et al., 1983: Reduction of systematic forecast errors in the ECMWF model through the introduction of envelope orography. *Quart. J. Roy. Met. Soc.*, **109**, 683–718.

Yanai, M. et al., 1973: Deformation of bulk properties of tropical cloud clusters from large–scale heat and moisture budgets. *J. Atmos. Sci.*, **30**, 611–627.

Zhang, Z. and T.N. Krishnamurti, 1997: On Ensemble Forecasting of Hurricane Tracks. *Bull. Amer. Meteor. Soc.*, **74**, 2785–2795.